P-29

SEMI-ANNUAL PROGRAM REPORT SUBMITTED TO NASA FOR GRANT #NAG5-1017

EVALUATION, DEVELOPMENT AND CHARACTERIZATION OF SUPERCONDUCTING MATERIALS FOR SPACE APPLICATIONS

by

Dr. Arthur N. Thorpe
Physics Department
Howard University
September, 1990

Anisotropic Electromagnetic Features of A Grain-aligned $YBa_2Cu_3O_x$ Bulk Superconductor

S. Hu, H. Hojaji, A. Barkatt, M. Boroomand

The Catholic University of America, Washington, D.C. 20064

A. N. Thorpe

Howard University, Washington, D.C. 20059

S. Alterescu

NASA Goddard Space Flight Center, Greenbelt, Maryland 20770

ABSTRACT The anisotropic electromagnetic features of a grain-aligned $YBa_2Cu_3O_x$ bulk sample derived from a process of long-time partial melt growth were investigated by the measurements of d.c. magnetization (at 77 k) and a.c. susceptibility as a function of temperature, with the fields applied parallel and perpendicular to the c axis, respectively. The extended Bean model was further studied and applied to explain the experimental results. Upon comparison of the grain-aligned sample with pure single crystal materials, it is concluded that because of the existence of more effective pinning sites in the grain-aligned sample, not only its critical current density perpendicular to the c axis is improved, but the one parallel to the c axis is improved even more significantly. The anisotropy in the critical current densities in the grain-aligned sample at 77 K is at least one to two orders of magnitude smaller than in the pure single crystal. The measurement of anisotroy of a.c. susceptibility as a function of temperature, especially its imaginary part, shows that there are still some

residues of interlayer weak links in the grain-aligned samples, but they are quite different from and far less serious than the weak links in the sintered samples.

1. INTRODUCTION

It has already been found that the single crystal $YBa_2Cu_3O_x$ superconductors have strong anisotropy in electromagnetic features.[1,2] However, for bulk samples produced exclusively by solid-state sintering (SSS), a macroscopic electromagnetic anisotropy cannot be specified because of the random orientations of the grains and the weak links between the grains.[3] Recently, however, several new methods to make the bulk $YBa_2Cu_3O_x$ sample, such as the methods of partial melt growth under temperature gradient,[4] long-time partial melt growth without temperature gradient,[5,6] and melt quenching followed by partial melt growth,[7] have been developed. With these methods it is now possible to cause the grains in the polycrystalline bulk sample to grow to a large size and to produce an aligned layer structure with the layers overlapping along their c axis. The current study focuses on the electromagnetic anisotropy of such grain-aligned (GA) $YBa_2Cu_3O_x$ bulk samples. This study is very important for the further understanding of the superconductivity of such materials and for the design of devices based on their use.

The measurement of d.c. magnetization has been widely used to

investigate the average effect of the pinning forces in type-II superconductors.[8] Characterization of the hysteresis loop permits calculation of the critical current density as a function of the applied field, especially in high field, based on Bean's model,[9] whenever the proper dimension of the superconducting structure can be specified. The measurement of the complex a.c. susceptibility as a function of the temperature and the applied field may offer more detailed information about inhomogeneity and coupling effects in superconductivity,[10-16] and some theoretical models of a.c. susceptibility are also presented[17-19]. But the anisotropic effects in bulk samples are always neglected in these studies.

In this paper we present the measurements of the d.c. magnetization at 77 K and the a.c. susceptibility as a function of temperature, with the applied magnetic field parallel or perpendicular to the c axis of the GA sample. In order to make use of Bean's model in fitting the results obtained for this bulk sample we further studied the extended form of this model.[20] It will be shown that this further study is helpful in understanding the electromagnetic anisotropy of GA $YBa_2Cu_3O_x$ bulk superconductors.

2. EXPERIMENTAL

The GA $YBa_2Cu_3O_x$ bulk samples were prepared by a method very similar to the one of long-time partial melt growth.[5,6] According to this method, a pre-sintered $YBa_2Cu_3O_x$ disc with a diameter of 10 mm

was rapidly heated to a temperature of about 1,100 °C and held for 20 min to form a mixture of Y_2BaCuO_5 and a liquid phase. It was then rapidly cooled to 1,040 °C, followed by cooling at a rate of 1 °C/hr to 970 °C to induce the peritectic conversion to $YBa_2Cu_3O_7$. It was then slowly cooled down to a temperature between 600 - 400 °C under oxygen to complete the tetragonal - orthorhombic phase transition. The SSS sample was made by sintering at 960 K for 24 hours followed by the same cooling process as the one used with the GA sample.

SEM studies[2] show that the GA sample obtained according to the method detailed above consists of various domains, which may range in size up to approximately 3x3x4 mm^3. Within each domain, the grains are layer-shaped with an average thickness of about 12 um. The $YBa_2Cu_3O_7$ layers, which are parallel to the ab plane, are densely packed along the common c axis of their particular domain. One large domain was chosen and cut to produce a cube with an edge dimension of 1.8 mm while making sure that one of the principal axes of the cube matches the c axis.

The d.c. magnetization was measured using a PARC vibrating sample magnetometer with the applied field either parallel to the c axis or perpendicular to the c axis. The sample was cooled to 77 K in zero field, and data were obtained as the field changed in increments of 20 Oe for the virgin magnetization curves, and 100 Oe for the rest. After each field increment, measurements were taken with a 2-minute delay to allow the sample to reach the critical state.[3]

The a.c. susceptibility was measured using a modified Hartshorn type a.c. mutual inductance bridge.[10,22] The a.c. bridge was calibrated to yield the real part of the a.c. susceptibility $4\pi\chi'$ = 0 and the imaginary part $4\pi\chi''$ = 0 by balancing the bridge at 105 K; and to yield $4\pi\chi'$ = -1 by cooling the GA sample to 77 K with a low a.c. field (0.05 Oe) parallel to the c axis. We believe this is a reasonable approximation since the $4\pi\chi'$ curve has already become very flat after the temperature drops below 85 K. The measurements were carried out with different applied fields which were either parallel or perpendicular to the c axis, while the temperature was lowered at a rate of 10 °C/hr. For all these measurements, the frequency of the applied fields was fixed at 45 Hz.

3. RESULTS AND DISCUSSION

3.1 Anisotropic d.c. magnetization

For the GA $YBa_2Cu_3O_x$ bulk sample, the results of measurement of the d.c. magnetization after the correction of the demagnetizing effect are shown in Fig. 1. From the hysteresis loops, with a maximum applied field H_{max} = 11 kOe and at T=77 K, the remnant magnetization M_r values are 61 and 16.5 emu/cm^3, and the widths of the hysteresis loops, ΔM, at a field 8 kOe, are 78 and 7.5 emu/cm^3, in the cases of the applied field being parallel or perpendicular

to the c axis, respectively. However, in the case of the sintered $YBa_2Cu_3O_x$ samples at T=77 K, M_r hardly reaches 1 emu/cm^3 and ΔM is of the order of 0.01 emu/cm^3 at H=8 kOe.[10,23] The reason for this dramatic difference between the GA sample and the SSS sample may be qualitatively explained by Bean's model. Based on this model, the magnetization curve is mainly correlated to the critical current density J_c and the effective thickness d_e of the sample, i.e., as expressed by,

$$\Delta M = \frac{1}{2c} J_c d_e \qquad (1)$$

where c is the speed of light. Eq. 1 and all the following equations are in cgs units unless otherwise specified. The SSS sample has serious weak links at the grain bouncaries, which cannot support a large J_c across them, although the J_c inside each grain is still very high.[23] Accordingly, the effective thickness of the SSS sample is almost as small as the thickness of the grains, about 2 - 10 um, at T $\approx$ 77 K and $H_{irr.} \approx$ 11 kOe. This is why SSS samples always show very small hysteresis loops. Conversely, the large hysteresis loops in Fig. 1 suggest that a large J_c must flow almost through the whole GA sample, even in the case of H $\perp$ c axis, since its corresponding ΔM at H = 8 kOe is still almost 3 orders larger than that of the SSS sample. Accordingly, the effective thickness of the GA sample is almost as same as its real thickness, at least for the cases of T $\leq$ 77 k and $H_{irr.} \leq$ 11 kOe.

In order to understand better the anisotropic electromagnetic

features of our cube-shaped sample, we did some further studies on the correlations between ΔM and H, H_{max}, the anisotropic critical current densities and the effective thicknesses, based on Bean's model and its extended form (see the appendix). The results are shown as follows.

When $H_{max} \leq H_{px}$,

$$\Delta M = (H_{max}^2 - H^2)\frac{1}{8\pi}\left(\frac{1}{H_{px}} + \frac{1}{H_{py}} - \frac{H_{max}}{H_{px}H_{py}}\right) \qquad (2)$$

when $H_{px} < H_{max} \leq 2H_{py}$, $|H| \leq 2H_{px} - H_{max}$,

$$\Delta M = \frac{1}{4\pi}\left(2H_{max} - H_{px} - \frac{1}{2}\left(\frac{1}{H_{px}} + \frac{1}{H_{py}}\right)(H_{max}^2 + H^2) + \frac{1}{3}\frac{H_{px}^2}{H_{py}} + \frac{1}{6}\frac{H_{max}}{H_{px}H_{py}}(H_{max}^2 + 3H^2)\right) \qquad (3)$$

when $H_{px} < H_{max} \leq 2H_{py}$, $|H| > 2H_{px} - H_{max}$,

$$\Delta M = \frac{H_{max} - H}{4\pi}\left(1 - \frac{1}{4}(H_{max} - H)\left(\frac{1}{H_{px}} + \frac{1}{H_{py}}\right) + \frac{1}{12H_{px}H_{py}}(H_{max} - H)^2\right) \qquad (4)$$

when $2H_{py} < H_{max}$, $|H| \leq H_{max} - 2H_{px}$,

$$\Delta M = \frac{H_{px}}{4\pi}\left(1 - \frac{1}{3}\frac{H_{px}}{H_{py}}\right) \qquad (5)$$

when $2H_{py} < H_{max}$, $|H| > H_{max} - 2H_{px}$,

$$\Delta M = \frac{H_{max}-H}{4\pi}\left(1-\frac{1}{4}(H_{max}-H)\left(\frac{1}{H_{px}}+\frac{1}{H_{py}}\right)+\frac{1}{12H_{px}H_{py}}(H_{max}-H)^2\right) \qquad (6)$$

Here, we assume that the applied field is along the z axis, and $H_{px} \leq H_{py}$. H_{px} and H_{py} are the penetrating fields through the x axis and the y axis, respectively, and they are expressed as,

$$H_{px} = \frac{2\pi}{C} J_c^y d_x \qquad (7)$$

$$H_{py} = \frac{2\pi}{C} J_c^x d_y \qquad (8)$$

where J_c^x and J_c^y are the critical current densities, and d_x and d_y are the effective thicknesses along the x axis and the y axis, respectively.

In the case of $H_{max} \gg H_{px}$, eq. 5 is suitable nearly for all $|H| < H_{max}$. If one converts the unit of J_c into A/cm^2, eq. 5 becomes

$$\Delta M = \frac{J_c^y d_x}{20}\left(1-\frac{1}{3}\frac{J_c^y d_x}{J_c^x d_y}\right) \qquad (9)$$

and this is the same as the expression first derived by Gyorgy *at al.*[20], except that they define d_x and d_y as the actual dimensions of a single crystal. But when it is applied to polycrystalline samples here, we regard them instead as effective thicknesses.

In the case of H ∥ c axis, the induced supercurrent is parallel to the ab plane, $J_c^x \approx J_c^y$, and $d_x \approx d_y$. In this case, based on eq. 9 we have

$$\Delta M = \frac{1}{30} J_c^{ab} d \qquad (10)$$

where J_c^{ab} is the critical current density parallel to ab plane, and d is the dimension of the cubic sample. With d = 0.18 cm, ΔM = 78 emu/cm^3 at H = 8 KOe and T = 77 K, we get $J_c^{ab} = 1.3 \times 10^4$ A/cm^2. This is about twice as large as that of the pure single crystal sample.[2]

In the case of H ⊥ c axis, not only J_c^{ab}, but also J_c^c, the critical current density along the c axis, is involved. In this case, eq. 9 can be properly rearranged as

$$\Delta M = \frac{J_c^c d}{20}\left(1 - \frac{1}{3}\frac{J_c^c}{J_c^{ab}}\right) \qquad (11)$$

Gyorgy *et al.* argued that when H⊥c the critical currents along the ab plane may be different depending on the flux vortices' moving direction with respect to the orientation of the twin boundaries.

But meanwhile they, and later Swartzendruber *at al.*[24], both found that the influence of twin boundaries on the pinning force is small, though measurable. If we further assume that the critical current along the ab plane will not be influenced significantly by the interlayer boundaries as these boundaries are parallel to the ab plane in the GA sample, then we can use the same J_c^{ab}, as we obtained above with H ∥ c, to estimate J_c^c. With ΔM = 7.6 emu/cm^3 at H = 8 KOe and T = 77 K, we have $J_c^c = 8.7 \times 10^2$ A/cm^2.

The anisotropy in the critical current density (ACCD), expressed as J_c^{ab} / J_c^c, is about 15 here for our GA cubic sample at T = 77 K and H = 8 KOe. Dinger *et al.*[1] have reported that for the pure single crystal $YBa_2Cu_3O_x$ sample at T = 40 K and H = 8 KOe, the ACCD is at least as high as 175, and it increases considerably at higher temperature and fields. Based on this, it is clear that at T ≈ 77 K, and H ≈ 8 KOe here, the ACCD of our GA sample is at least one to two orders of magnitude smaller than that of the pure single crystal. It appears that long-time partial melt growth induces, in addition to grain alignment, the presence of more effective flux pinning sites inside the sample. Because of these pinning sites, not only the J_c^{ab} value increases, but the J_c^c value increases even more significantly comparing with the J_c^{ab} and J_c^c values, respectively, of the pure single crystal. The exact nature of pinning sites introduced here and the mechanism of their pinning activity are still open questions. One of the possibilities may be that as a result of long-time partial melting some part of the liquid phase, as we have actually observed, separates and flows

away. Consequently some fine pores and some fine grains of phases with higher melting points, such as Y_2BaCuO_5, remain trapped inside the sample with a fairly uniform distribution. Such pores or second-phases may serve effectively as pinning sites.

3.2 Anisotropic a.c. susceptibility

In the case of the applied a.c. field, $H_{ac}(t) = h_c\cos(\omega t)$, being parallel to the c axis, the results of the a.c. susceptibility measurement for the GA sample are shown in Fig. 2. For comparison here, we show the results for the SSS sample in Fig. 3. For the GA sample, when the $4\pi\chi'$ drops from 0 to -0.5, the temperature changes 0.23, 0.29, 0.42 K, corresponding to h_c values of 0.15, 0.70, 1.25 Oe, respectively. The shift in $4\pi\chi' = 0.5$ is about 0.17 K/Oe, while for the SSS sample the temperature changes 0.9, 1.6, 2.9 K, respectively, and the shift is about 1.8 K/Oe. For the SSS sample, the $4\pi\chi'$ drops in two steps, the one at higher temperature corresponding to the intragrain transition, while the other one corresponding to the intergrain weak links.[10-19] The later one rapidly shifts to even lower temperature with slight increase in h_c. However for the GA sample, $4\pi\chi'$ only has one step of rapid drop and it appears much less sensitive to the applied fields, i.e. no weak link behavior is observed in this case. This can be confirmed more directly from the measurement results of the $4\pi\chi''$. Fig.3 (B) shows that for $4\pi\chi''$ of the SSS sample, its higher temperature (HT) peak appears right below T_c, and is very small, followed by a

very large lower temperature (LT) peak. The LT peak shifts to even lower temperature and becomes even broader very rapidly with slight increase in h_0. It is the very typical feature of the weak links. But for the GA sample, $4\pi\chi''$ in Fig. 2 (B) shows no sign of the existence of any LT peak. Besides, its HT peak is about one to two orders of magnitude higher than the corresponding one of the SSS sample. The disappearance of the LT peak further confirms the disappearance of the intralayer weak links in the GA sample, as in the case of $H_{ac} \parallel c$ no induced interlayer currents are involved. The large change in the HT peak must be caused mainly by the change in the effective thickness of the samples. The following considerations may help us to understand it better.

Since the a.c. susceptibility is measured at low frequency (45 Hz here), the dissipation of energy is mainly due to the hysteresis loss. Following the approach described in Ref. 15, the average magnetization M(t) is given by

$$M(t) = h_o \sum_n (\chi'_n \cos\omega t + \chi''_n \sin\omega t) \qquad (12)$$

and if one neglects the terms with n > 1 in this Fourier expansion, then $4\pi\chi''$ can be expressed as[15,13]

$$4\pi\chi'' = \frac{4}{h_o^2} \oint (-M)\, dH \qquad (13)$$

From eqs. 2 - 6, we get

$$\oint(-M)\,dH = \frac{1}{6\pi}h_o^3\left(\frac{1}{H_{px}}+\frac{1}{H_{py}}-\frac{h_o}{H_{px}H_{py}}\right), \qquad h_o \le H_{px} \tag{14}$$

and

$$\oint(-M)\,dH = \frac{1}{2\pi}h_oH_{px}\left(\left(1-\frac{2}{3}\frac{H_{px}}{h_o}\right)-\frac{1}{3}\frac{H_{px}}{H_{py}}\left(1-\frac{H_{px}}{h_o}\right)\right), \qquad h_o > H_{py} \tag{15}$$

J_c is a function of the temperature and may be usually expressed by

$$J_c(T) = (1-T/T_c)^n J_c(0) \tag{16}$$

where n is positive.[24] Accordingly,

$$4\pi\chi'' = \frac{ch_o}{3\pi^2 J_c^y d_x}\left(1+\frac{J_c^y d_x}{J_c^x d_y}-\frac{ch_o}{2\pi J_c^x d_y}\right), \qquad T \le T^* \tag{17}$$

and

$$4\pi\chi'' = \frac{4J_c^y d_x}{ch_o}\left(1 - \frac{4\pi J_c^y d_x}{3ch_o} - \frac{J_c^y d_x}{3J_c^x d_y}\left(1 - \frac{2\pi J_c^y d_x}{ch_o}\right)\right) \quad , \quad T^* < T < T_c \tag{18}$$

where T^* is the critical temperature, below which no magnetic flux can reach the center of the sample.

When $H_{ac} \parallel$ c axis, both J_c^y and J_c^x may be replaced by J_c^{ab}, then from eqs. 17 - 18 we can see that when the temperature decreases $4\pi\chi''$ increases mainly with $J_c^{ab}d_e$ if the temperature is between T^* and T_c, and $4\pi\chi''$ drops mainly with $1/J_c^{ab}d_e$ if it is below T^*. Assuming the intralayer J_c^{ab} of the GA sample and the intragrain J_c^{ab} of the SSS sample to be approximately the same, it can accordingly be expected that when the effective thickness d_e of a sample is larger, its HT peak should be sharper and higher. Because the SSS sample has serious intergrain weak links, its d_e right below T_c should not be much larger than the average thickness of its grains, and this is why its HT peak is much smaller and flatter compared with the HT peak of the GA sample. The latter shows no intralayer weak links and its d_e should almost be the same as its actual thickness.

In the case of $H_{ac} \perp$ c axis, $4\pi\chi'$, as shown in Fig. 4 (A),

drops from 0 to -0.55 almost as fast as it does when $H_{ac} \parallel c$, but below -0.55 the drop is apparently slower. The reason for this may be either that the c axis component of the intralayer pinning forces does not increase as fast as the ab-plane component does with decreasing temperature, or that there are still some residues of interlayer weak links. The measurements of $4\pi\chi''$ further confirm the existence of the residual interlayer weak links. Fig. 4 (B) shows that in this case $4\pi\chi''$ not only has a HT peak, which is almost the same as in the case of $H_{ac} \parallel c$ except for being slightly smaller, but also has a residue of the LT peak. Since in this case the magnetic flux is parallel to the layer-layer boundaries, the appearance of the residual LT peak suggests that some portion of the these boundaries are still relatively "weak". However, since the LP peak is only as high as about 1/3 of the HT peak in this case, while for the SSS sample the LT peak is about one to two orders higher than the HT peak, it is clear that the proportion of "weak" boundaries is very small for the GA sample. From eqs. 17, 18 and the similarity between the HT peaks in the cases of $H_{ac} \perp c$ and $H_{ac} \parallel c$, it seems that the layer-layer boundaries have, to a large extent, become fairly "strong" so as to support the induced current to cycle across them right below T_c. In other words, since these fairly "strong" boundaries connect the layers together, the effective thickness even in the c-axis direction is still almost the same as the actual thickness of the GA sample in the direction of interest. And the proportion of the "weak" boundaries is not only small, but they are also isolated inside the sample. This is

quite different from the situation in the case of the SSS sample, in which most of the grains are isolated by the weak links.

5. CONCLUSION

As a result of the long-time partial melt growth processing, a pre-sintered $YBa_2Cu_3O_y$ bulk sample becomes grain-aligned within domains with typical dimensions of 3x3x4 mm^3. At the same time some more effective pinning sites appear in such samples. Because of the presence of these pinning sites not only the critical current density perpendicular to the c axis is improved, but also the one parallel to the c axis. The improvement in the latter case is even more significant relative to values obtained with pure single-crystal $YBa_2Cu_3O_x$. For the grain-aligned sample studied here, there are still some residues of interlayer weak links, but these weak links are isolated and they constitute a far less serious problem than that in the case of the sintered sample.

The measurement of the anisotropy in a. c. susceptibility, especially its imaginary part, as a function of temperature and applied field is likely to be very helpful in investigating the degree with which the grains are aligned and the relative significance of the residual interlayer weak links in grain-aligned bulk superconductors.

Acknowledgement

This study was supported in part by the National Space and Aeronautics Administration under Contract no. NAG 5-1017.

Appendix

For a sample with a rectangular cross section $d_x \times d_y$ and infinitely long in z direction, following the same approximation as used in Ref.20 that the induced supercurrents flow along rectangular loops when the applied field is parallel to the z axis, one can find that the distribution of magnetic flux density B(x,y) in the case of $H_{max} \leq H_{p1}$ and H changes from H_{max} to $-H_{max}$ is, as illustrated in Fig. A1,

in S_1 ($0 \leq x \leq x_1$, $(J_c^y/J_c^x)x \leq y \leq d_y/2$),

$$B = H + (4\pi J_c^y/c)x \quad ; \tag{A1}$$

in S_2 ($x_1 \leq x \leq x_2$, $(J_c^y/J_c^x)x \leq y \leq d_y/2$),

$$B = H_{max} - (4\pi J_c^y/c)x \quad ; \tag{A2}$$

in S_3 ($x_2 \leq x \leq d_x/2$, $y_2 \leq y \leq d_y/2$),

$$B = 0 \quad ; \tag{A3}$$

in S_4 ($(J_c^x/J_c^y)y \leq x \leq d_x/2$, $y_1 \leq y \leq y_2$),

$$B = H_{max} - (4\pi J_c^x/c)y \quad ; \tag{A4}$$

in S_5 ($(J_c^x/J_c^y)y \leq x \leq d_x/2$, $0 \leq y \leq y_1$),

$$B = H + (4\pi J_c^x/c)y \quad , \tag{A5}$$

where,

$$x_1 = (H_{max} - H)/(8\pi J_c^y/c) \quad , \tag{A6}$$

$$x_2 = H_{max}/(4\pi J_c^y/c) \quad , \tag{A7}$$

$$y_1 = (H_{max} - H)/(8\pi J_c^x/c) \quad , \tag{A8}$$

$$y_2 = H_{max}/(4\pi J_c^y/c) \quad . \tag{A9}$$

The corresponding magnetization is

$$M^+ = (B - H)/(4\pi)$$

$$= \{ 4/(d_x d_y) * \Sigma \int B \, ds - H \}/(4\pi) \quad . \tag{A10}$$

When H changes from $-H_{max}$ to H_{max}, because of the symmetry of M-H loops, the corresponding magnetization is

$$M^-(H) = -M^+(-H) \quad . \tag{A12}$$

Then, $$\Delta M = M^+ - M^- \quad , \tag{A13}$$

which leads to Eq.2. Similarly one can also get Eqs.3-6 related to the cases of $H_{px} < H_{max} \leq 2H_{px}$ and $2H_{px} < H_{max}$.

REFERENCE

[1] T. R. Dinger, T. K. Worthington, W. J. Gallagher, and R. L. Sandstrom, Phys. Rev. Lett. **58**, 2687 (1987).

[2] G. W. Crabtree, J. Z. Liu, A. Umezawa, W. K. Kwok, C.H. Sowers, S. K. Malik, B. W. Veal, D. J. Lam, M. B. Brodsky, and J. W. Downey, Phys. Rev. B 36, 4021 (1987).

[3] J. W. Ekin, A. I. Braginki, A. J. Panson, M. A. Janocko, D. W. Capone, II, N. J. zaluzec, B. Flandermeyer, C. F. de Lima, M. Hong, J. Kwo, and S. H. Liou, J. Appl. Phys. **62**, 4821 (1987).

[4]S. Jin, T. H. Tiefei, R. C. Sherwood, M. E. Dvis, R. B. van Dover, G. W. Kammlott, R. A. Fastnacht, and H. D. Keith, Appl. Phys. Lett. 52, 2074 (1988).

[5]V. Salama, V. Selvamanickam, L. Gao, and K. Sun, Appl. Phys. Lett. 54, 2352 (1989).

[6]H. Hojaji, A. Barkatt, K. A. Michael, S. Hu, A. N. Thorpe, M. F. Ware, I. G. Talmy, D. A. Haught, and S. Alterescu, J. Mater. Res. 5, 721 (1990).

[7]M. Murakami, M. Morita, and N. Koyama, Jpn. J. Appl. Phys. 28, L1125 (1989).

[8]A. M. Campbell, and J. E. Evtts, Advan. Phys. 21, 199 (1972).

[9]C. P. Bean, Rev. MOd. Phys. 36, 31 (1964).

[10]R. A. Hein, H. Hojaji, A. Barkatt, H. Shafii, K. A. Michael, A. N. Thorpe, M. F. Ware, and S. Alterescu, J. Supercod. 2, 427 (1989).

[11]R. B. Goldfarb, A. F. Clark, A. I. Braginski, and A. J. Panson, Cryogenics 27, 475 (1987).

[12]K. V. Rao, D.-X. Chen, J. Nogues, C. Politis, C. Gallo, and J. A.

Gerber, in *High Temperature Superconductoors* (Materials Research Society, Pittsburgh, 1987), p. 133.

[13]Yu Mei, H. L. Luo, D.-X. Chen, J. Nogues, and K. V. Rao, J. Appl. Phys. **64**, 2533 (1988).

[14]R. B. Flippen and T. R. Askew, Solid State Commun. **72**, 337 (1989).

[15]V. Calzona, M. R. Cimberle, C. Ferdeghini, M. Putti, and A. S. Siri, Physica C **157**, 425 (1989).

[16]K.-H. Muller and A. J. Pauza, Physica C **161**, 319 (1989).

[17]J. R. Clen, Physica C **153-155**, 50 (1988).

[18]D.-X. Chen, J. Nogues, and K. V. Rao, Cryogenics **29**, 800 (1989).

[19]K.-H. Muller, Physica C **159**, 717 (1989).

[20]E. M. Gyorgy, R. B. van Dover, K. A. Jackson, L. F. Schneemeyer, and J. V. Waszczak, Appl. Phys. Lett. **55**, 283 (1989)

[21]H. Hojaji, S. Hu, K. A. Michael, A. Barkatt, A. N. Thorpe, and S. Alterescu, to be published in Proc. of Advances Materials Science and Applications of High Temperature Superconductors, April 2-6, 1990, Greenbelt, MD.

[22]R. A. Hein, Phys. Rev. B 33, 7539 (1986).

[23]S. Jin, R. C. Sherwood, E. M. Gyorgy, T. H. Tiefel, R. B. van Dover, S. Nakahara, L. F. Schneemeyer, R. A. Fastnacht, and M. E. Davis, Appl. Phys. Lett. **54**, 584 (1989).

[24]L. J. Swartzendruber, A. Roitburd, D. L. Kaiser, F. W. Gayle, and L. H. Bennett, Phys. Rev. Lett. **64**, 483 (1989).

[25]Y. Yeshuran, A. P. Malozemoff, and F. Holtzberg, J. Appl. Phys. **64**, 5797 (1988).

Captions

Fig.1. Magnetization hysteresis loops at 77 K for the grain-aligned sample with the c axis oriented (a) parallel to the applied field and (b) perpendicular to the applied field.

Fig.2. (A) Real part and (B) Imaginary part of the a.c. susceptibility as a function of temperature for the grain-aligned sample with various a.c. magnetic fields applied parallel to the c axis.

Fig.3. (A) Real part and (B) Imaginary part of the a.c. susceptibility as a function of temperature for the sintered sample with various applied a.c. magnetic fields.

Fig.4. (A) Real part and (B) Imaginary part of the a.c. susceptibility as a function of temperature for the grain-aligned sample with various a.c. magnetic fields applied perpendicular to the c axis.

Fig.A1. Distribution of $B(x,y)$ ($H_{ma} \leq H_{p}$).

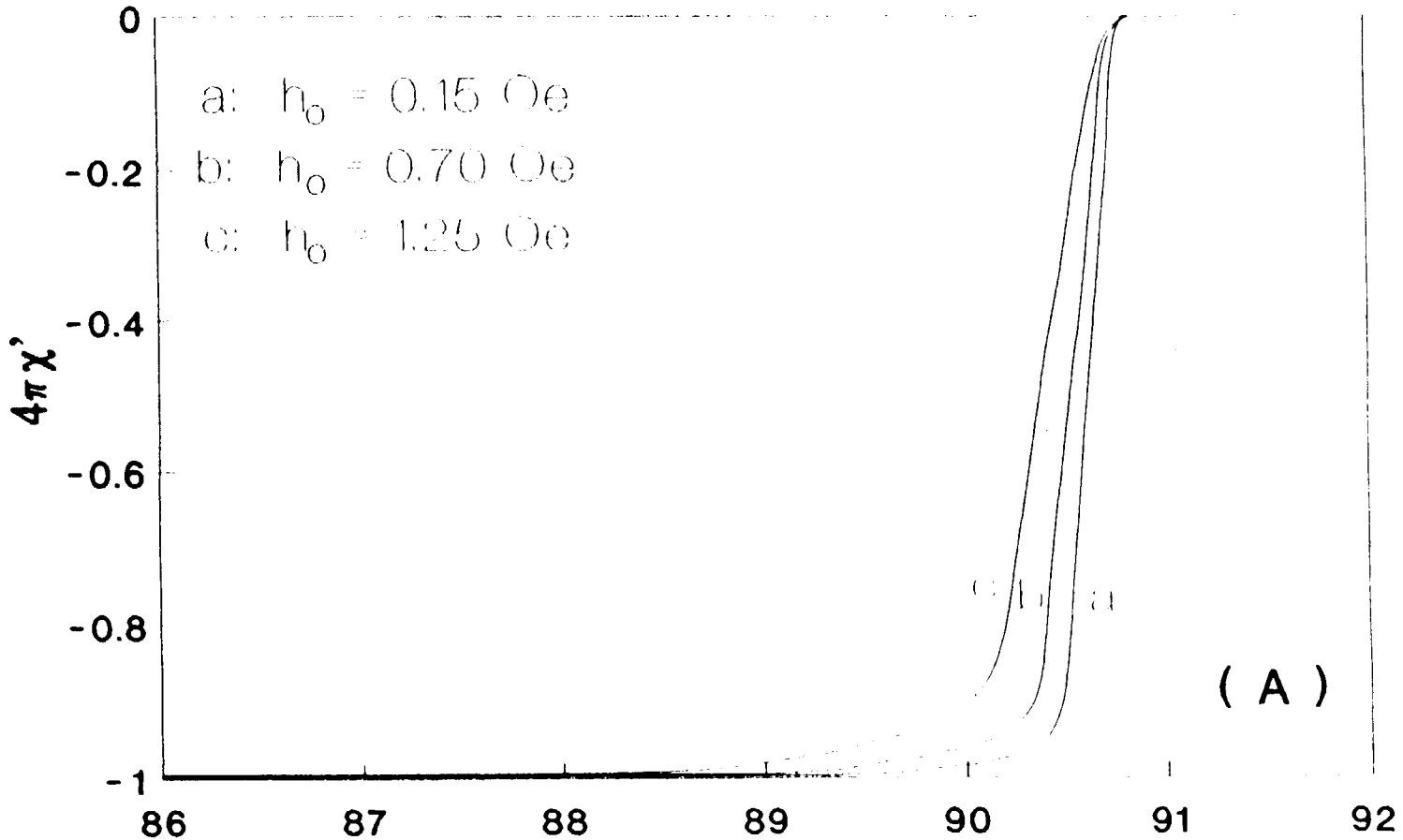

Fig. 2 (A

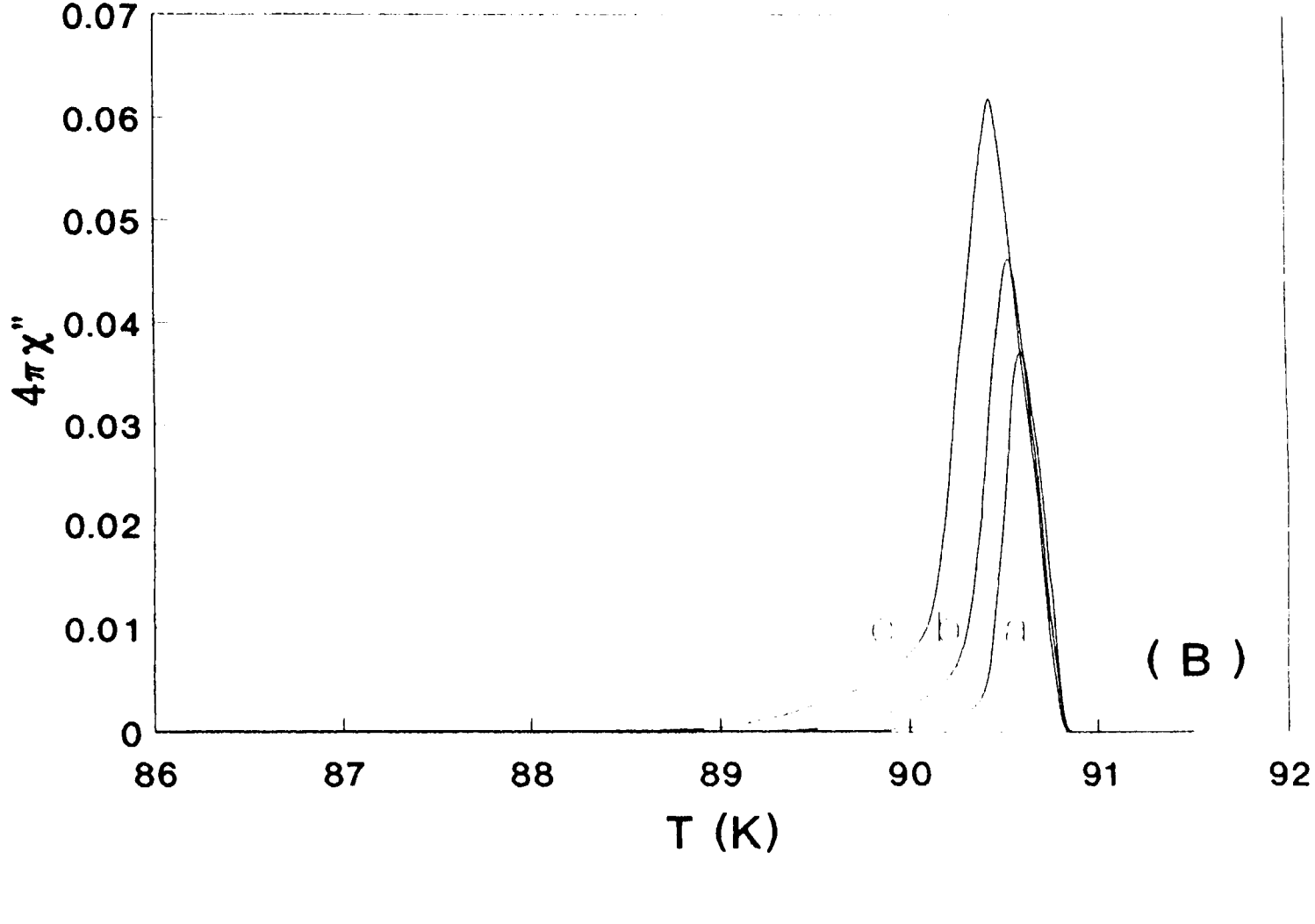

Fig. 2 (

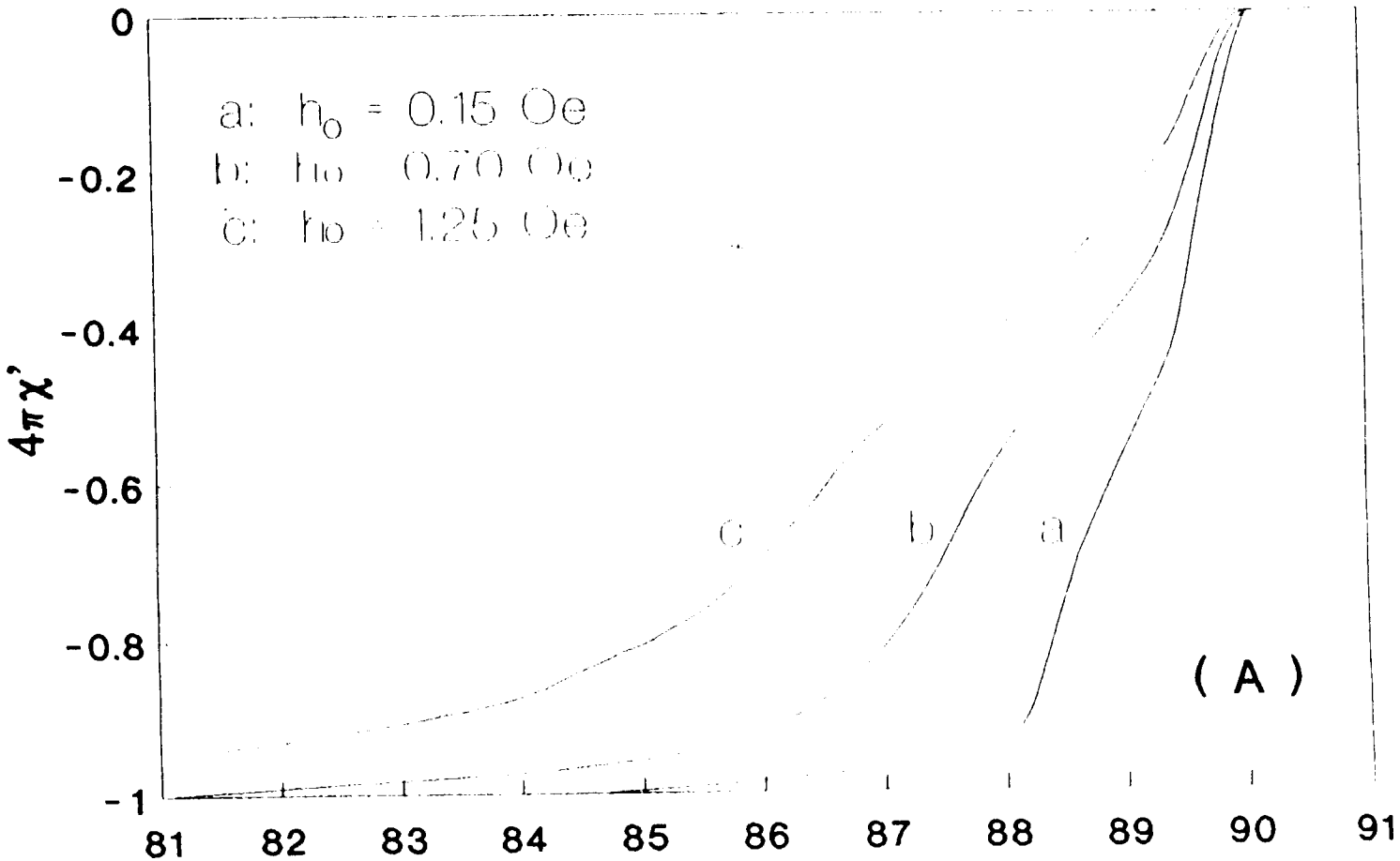

Fig. 3 (A)

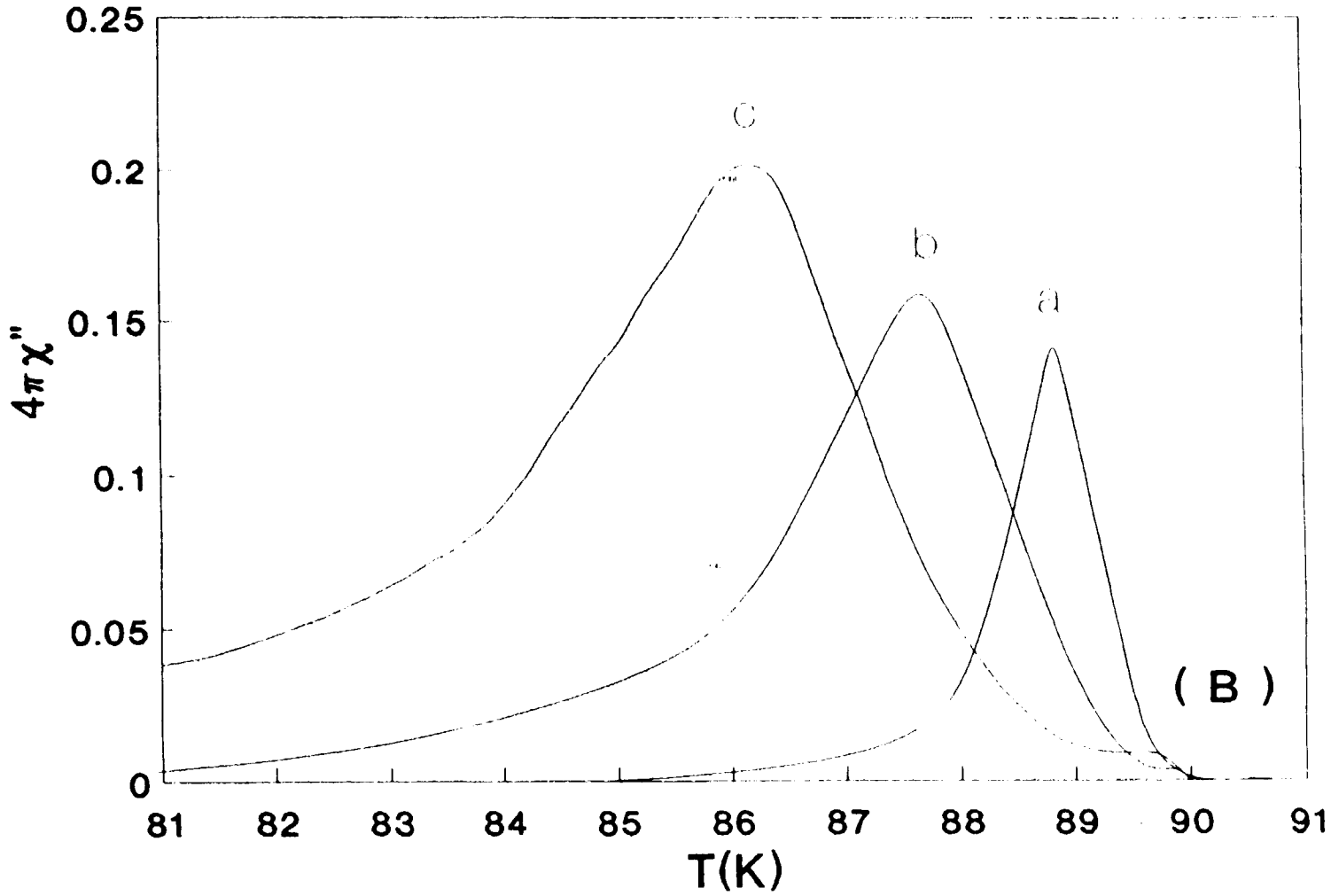

Fig. 3 (B)

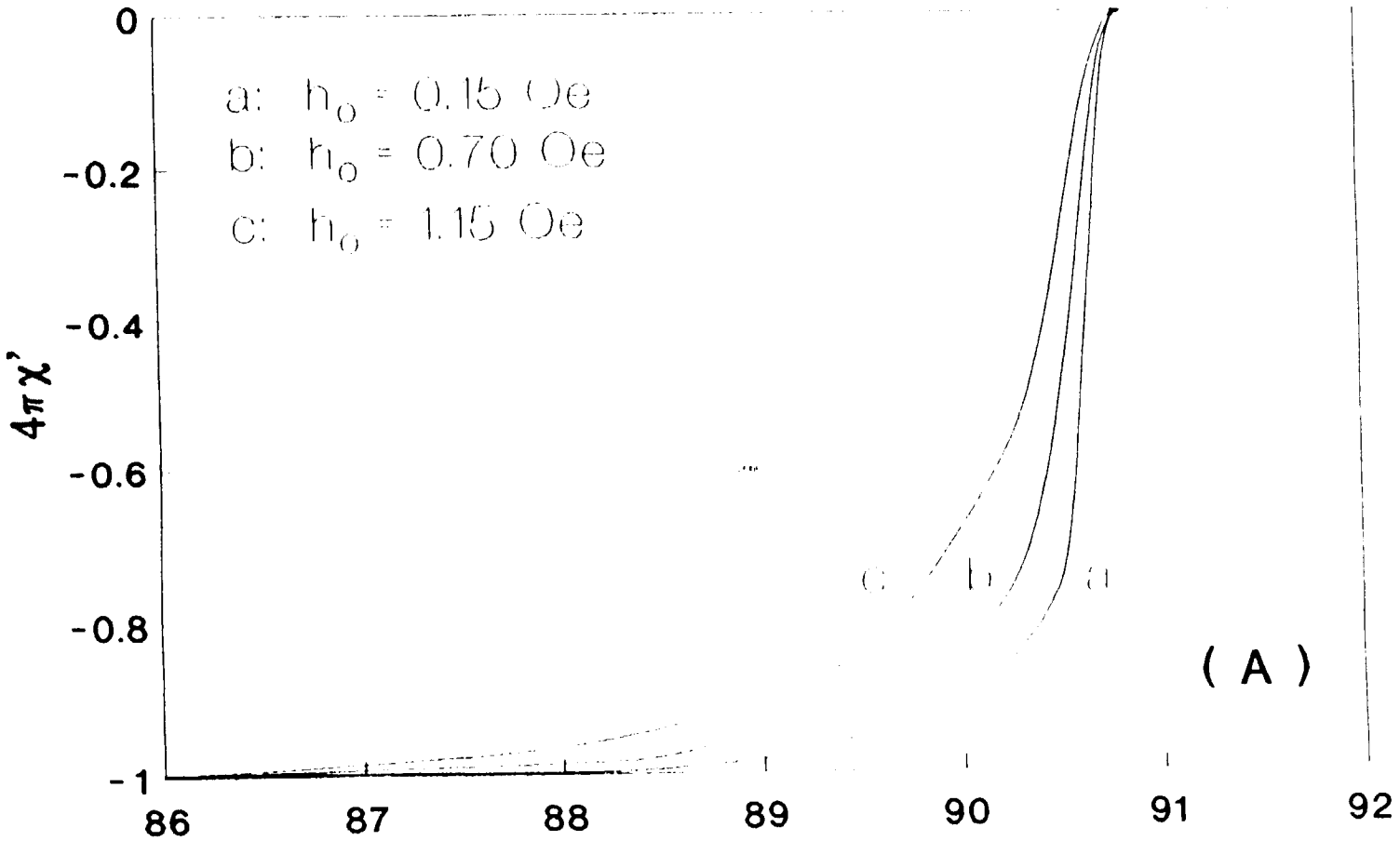

Fig. 4. (A)

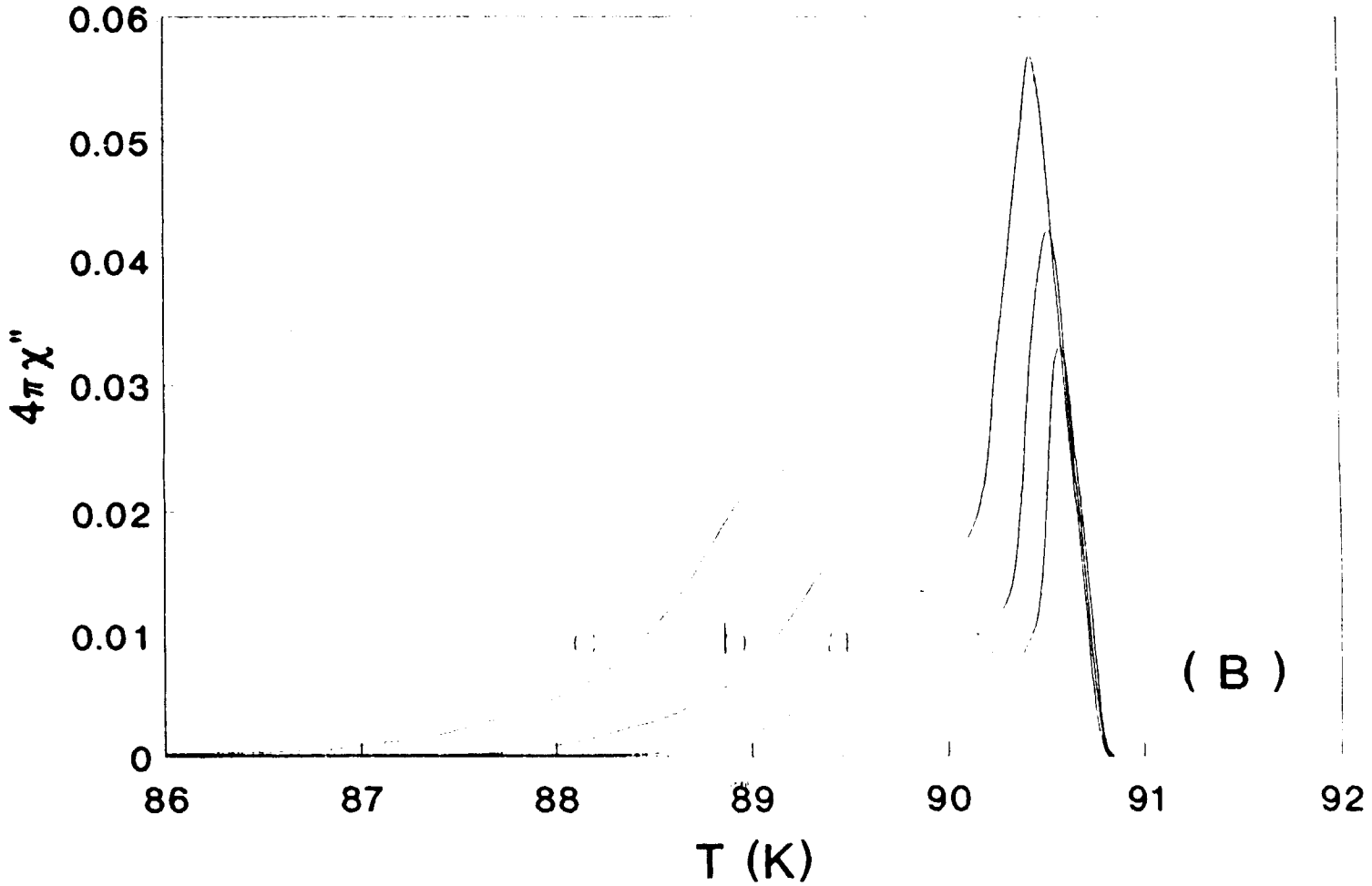

Fig 4 (B)